به نام خدا

مرکز دانلود رایگان
مهندسی متالورژی و مواد

www.Iran-mavad.com

3
Kinetics of martensite transformations in steels

G. B. OLSON and Z. D. FEINBERG,
Northwestern University, USA

Abstract: Dislocation theory of the mechanism and kinetics of martensitic transformation has provided a foundation for the prediction of constitutive relations for transformation plasiticity. Application to the control of stress-state dependent shaping of stress–strain behavior has demonstrated substantial improvements in uniform ductility and ductile fracture toughness. The advance of such predictive science continues to play a central role in the new enterprise of science-based materials design.

Key words: martensitic transformation, transformation kinetics, transformation plasticity, transformation toughening.

3.1 Introduction

A martensitic phase transformation can be considered as the spontaneous plastic deformation of a crystalline solid in response to internal chemical forces. It is no surprise, then, that the theory of dislocations, after incorporating the generalized forces of chemical thermodynamics and special constraints of crystalline interfaces, has provided the most useful basis for understanding the mechanism of these transformations. Martensitic transformations have been defined as a subset of diffusionless/displacive solid-state transformations in which the strain energy arising from a shear-dominant lattice distortion controls the kinetics and product morphology during transformation (Christian *et al.*, 1995). Such transformations are first-order and heterogeneous in nature, proceeding by the propagation of relatively sharp interfaces. These characteristics make the approximations of traditional linear-elastic dislocation theory particularly appropriate, and it is for this reason that the application of the theory to martensitic transformations (Olson and Cohen, 1986a) has been so successful.

These same characteristics give rise to the high mobility of martensitic interfaces underlying the quench-hardening of steel and the precisely prescribable transformation kinematics predicting their interaction with applied stress exploited in transformation plasticity applications. The latter applications span not only modern TRIP (transformation-induced plasticity) steels, but the still emerging class of shape memory alloys.

59

3.2   Mechanism and kinetics of martensitic transformation

The application of classical nucleation theory to martensitic transformations, using both continuum-elastic and discrete-dislocation descriptions of a nucleus, has been extensively reviewed (Olson and Cohen, 1981, 1982, 1986a). The classical approach treats the energetics of formation of a nucleus along a 'path' of fixed structure and increasing size. The nucleus crystal structure is taken to be that of the fully formed transformation product, with relatively sharp interface; the specific interfacial energy is customarily assumed to be size independent.

The specific interfacial energy γ of a fully coherent particle will consist of a 'chemical' core energy, while the interfacial energy in the semi-coherent case will be dominated by a short-range elastic-energy contribution. If the nucleus transformation strain (IPS) is an invariant-plane strain, the strain energy per particle volume for a thin oblate spheroid of radius r and semi-thickness c is of the form Kc/r, where K is an elastic constant. When the transformation strain deviates from an exact invariant-plane strain, an additional shape-insensitive strain energy contribution g_p^{str} arises from distortions in the particle habit plane. Following Kaufman and Cohen (1958), the total free energy of an isolated martensitic particle can thus be described by:

$$\Delta G(r, c) \quad \blacksquare \quad \frac{4}{3} \quad \blacksquare \quad ^2 \quad \blacksquare \quad \frac{4}{3}\pi r^2 K + 2\pi r^2 \gamma \qquad [3.1]$$

Under the thermodynamic conditions for which martensitic transformations are known to occur, the critical energy barrier is far too large to be thermally surmountable, and it can be safely concluded that classical homogeneous nucleation is not possible.

In an imperfect crystal, defect interactions can substantially alter the energy of a classical nucleus such that the free-energy barrier for heterogeneous nucleation is greatly diminished relative to the homogeneous case. Consistent with the strain-energy dominant character of martensitic transformations, it is generally assumed that the most important interaction in heterogeneous martensitic nucleation is with the defect stress field. It is now well established by quantitative calculations that classical nucleation via such interaction is indeed quite plausible at experimentally observed heterogeneous nucleation sites. While this interaction can be described by traditional continuum-elastic methods, the structurally equivalent discrete-dislocation description in terms of a defect-dissociation process leads most directly to the essential behavior, and is actually the method by which the first viable theory of heterogeneous martensitic nucleation was developed (Olson and Cohen, 1976a, 1976b).

3.2.1   Heterogeneous nucleation by defect dissociation

Adopting the discrete-dislocation description of Fig. 3.1 for the interfacial structure of a classical martensitic embryo, the long-range stress field and volume strain energy of the embryo arise primarily from the array of transformation 'coherency' dislocations lying on crystal planes at a shallow angle to the embryo habit as represented schematically in Fig. 3.1(a). Clearly the free-energy barrier for nucleation is greatly diminished if the latter dislocation array is derived from the dissociation of an existing defect. A convenient defect model for this purpose is the extrinsic boundary defect represented by the array of 'excess' interfacial dislocation in Fig. 3.2(a), residing in an existing grain boundary or interphase boundary. The defect has a finite length and height, and a net Burgers vector content giving rise to a stress field of range comparable to its length, l. Embryo formation by dissociation of this defect is depicted in Figs 3.2(b) and (c). The interfacial motion producing such a particle involves both the motion of the array of Fig. 3.1(a) as shown in Fig. 3.2(b), and the sequential formation of the discrete loops in Figs 3.1(b) and (c) under the acting thermodynamic driving force, represented by Fig. 3.2(c).
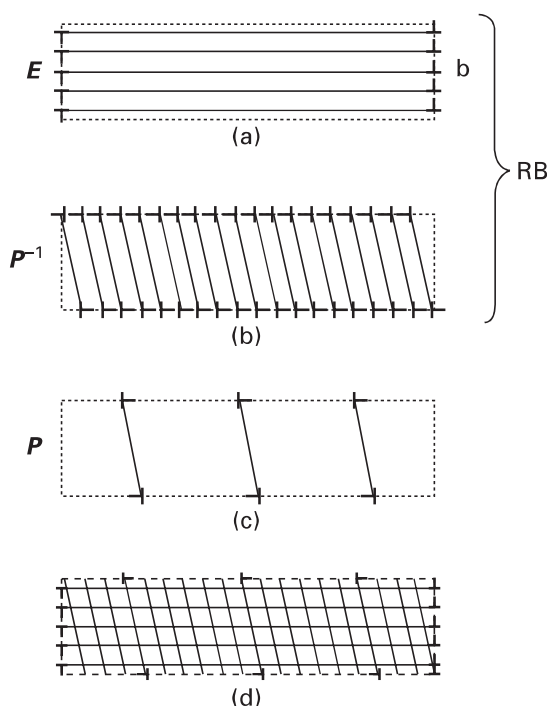
3.1 Discrete-dislocation model of martensitic interface: (a) transformation 'coherency' dislocations producing macroscopic shape strain **E**; (b) coherency dislocations producing complementary shear **P**$^{-1}$; (c) anticoherency dislocations producing lattice-invariant deformation **P**; (d) total interfacial structure (Olson and Cohen, 1981a).
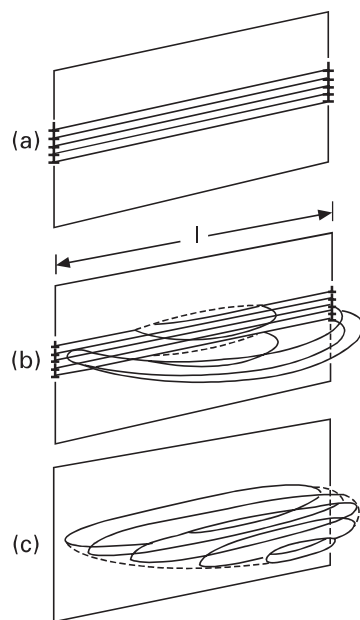
3.2 Heterogeneous martensitic nucleation by defect dissociation: (a) nucleating defect; (b) dissociation to produce interfacial coherency dislocations of Fig. 3.1(a) in horizontal planes; (c) simultaneous generation of interfacial dislocation arrays of Figs 3.1(b) and (c) in nearly vertical planes (Olson and Cohen, 1981a).

Following prediction of interfacial structure theory that the most significant coherency dislocations will be associated with planes of closest packing, it is appropriate for the construction of the dislocation arrays of Figs 3.1(a) and (b) to decompose the transformation lattice deformation into invariant-plane strains on close-packed planes. For face-centered cubic (fcc) to body-centered cubic (bcc) transformation as in ferrous alloys, such a decomposition was proposed by Bogers and Burgers (1964) based on a hard-sphere deformation model. The resulting specific model for a martensitic nucleus provided the basis for the first detailed quantitative treatment of the energetics of classical heterogeneous nucleation. This model has predicted the essential characteristics of barrierless heterogeneous nucleation of martensitic transformations, with kinetic control by interfacial mobility. Combined with treatment of the composition dependence of solution hardening effects on the interfacial mobility, it has provided the framework for the most accurate prediction of the critical driving force for martensitic nucleation in complex alloys (Ghosh and Olson, 1994a, 1994b). Using a distribution of total Burgers vector content for 'superdislocation' defects of the type of Fig. 3.2(a) to describe potency distributions of both pre-existing defects and new 'autocatalytic' defects generated by martensite growth events, it has also provided the basis for a kinetic theory of the full evolution of martensitic transformations (Lin *et al.*, 1992). Incorporating both athermal and thermal components of the martensitic

interfacial mobility, the general theory accounts for both systems exhibiting 'athermal' (time-independent) behavior and the so-called 'isothermal' (time-dependent) mode of behavior, depending on the relative magnitude of the thermal terms in the interfacial mobility.

3.3 Mechanically induced transformations

Applied stress can assist the operation of the same nucleation sites (with the same total critical driving force) responsible for the transformation on cooling; such stress-assisted nucleation can be described for any stress state by the thermodynamic effect of stress as first derived by Patel and Cohen (1953):

$$\Delta g^{\sigma} = \tau \gamma_T + \sigma_n \varepsilon_n, \qquad [3.2]$$

where τ and σ_n are the resolved shear and normal stresses in the planes and directions of the transformation shear (γ_T) and normal strain (ε_n). However, if the applied stress exceeds the yield stress of the parent phase, strain-induced nucleation can occur on new potent nucleation sites created by the plastic strain. Under these circumstances, nucleation sites are plentiful, and this has allowed numerous detailed observations of strain-induced sites, consisting primarily of various types of shear-band intersections, and including intersections with grain boundaries (Venables, 1962; Lagneborg, 1964; Manganon and Thomas, 1970; Lecroise and Pineau, 1972; Suzuki *et al.*, 1977; Brooks *et al.*, 1979). The shear bands may be mechanical twins, hexagonal close-packed (hcp) ε-martensite, bundles of stacking faults, or slip bands. In each case, the intersection can be interpreted as producing a dislocation stacking of the type illustrated in Fig. 3.2(a), and the relation of the active displacement to the orientation variant of the martensite being formed is consistent with the defect dissociation model (Lecroise and Pineau, 1972; Suzuki *et al.*, 1977; Brooks *et al.*, 1979). More potent defects can be generated in this way, compared to those existing in the annealed parent phase, and hence strain-induced nucleation can occur at lower driving forces.

The temperature regimes in which transformation initiates predominantly from either stress-assisted or strain-induced nucleation are depicted in the schematic stress–temperature diagram of Fig. 3.3. Spontaneous transformation triggered by existing nucleation sites occurs on cooling to the martensite start (M_s) temperature. Stress-assisted nucleation on the same sites will occur at the stress denoted by the solid line indicated. At a temperature designated M_s^{σ}, this stress reaches the yield stress σ_y for slip in the parent phase. Above M_s^{σ}, new potent nucleation sites introduced by plastic strain trigger strain-induced nucleation at the stress level depicted by the indicated solid curve. The temperature M_s^{σ} thus defines an approximate boundary between the temperature regimes where the two modes of nucleation dominate; near
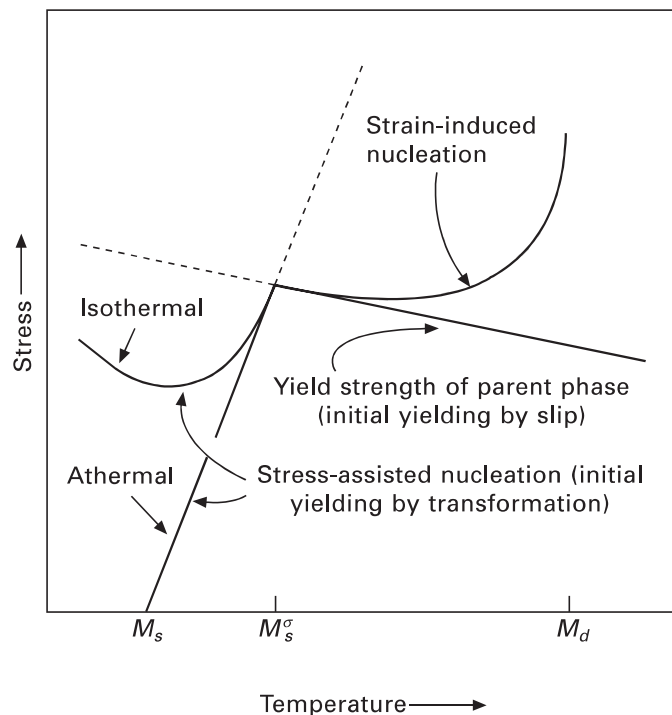
3.3 Schematic representation of interrelationships between stress-assisted and strain-induced martensitic transformation (Olson and Cohen, 1972).

M_s^σ both modes will operate. Due to transformation plasticity, the observed yield stress follows the stress for stress-assisted transformation below M_s^σ. A reversal of the temperature dependence of the yield stress thus provides a convenient determination of the M_s^σ temperature. Above the temperature M_d, no transformation occurs on deformation to fracture. Figure 3.3 represents the behavior for a particular stress state.

3.3.1   Mechanism of stress-assisted transformations

Using the Patel–Cohen model (Patel and Cohen, 1953) of Eq. [3.2] for the work of applied stress computed for the most favorably oriented martensitic plate, the calculated driving force contribution of applied stress in uniaxial tension ($\partial \Delta G/\partial \sigma$) is in good agreement with the observed stress dependence of the M_s temperature in alloys exhibiting nominally athermal kinetic behavior (Patel and Cohen, 1953; Bolling and Richman, 1970; Fisher, 1974). In addition to the numerous studies of the stress dependence of the M_s temperature, the stimulating influence of applied stress on the rate of the time-dependent isothermal transformation was first demonstrated by Machlin and Cohen (1952).

The macroscopic transformation plasticity accompanying the transformation can arise in part from a biasing of the martensitic-plate variants which form

under stress, but in ferrous alloys (particularly when a strong autocatalytic effect operates), much of the transformation plasticity is attributable to stress biasing of the extensive accommodation slip which occurs around the plates as they grow. When this deformation takes place at stresses below that for general (slip) yielding of the parent phase (i.e., the temperature regime where stress-assisted transformation is dominant), the kinetics of the transformation paces the macroscopic deformation. The simultaneous measurement of plastic flow and transformation in TRIP steels (Olson and Azrin, 1978) verifies the existence of a temperature regime in which plastic flow is controlled by stress-assisted martensitic transformation. Under these conditions, the volume fraction of martensite (f) and the plastic strain (ε) are confirmed to be linearly related (Olson and Azrin, 1978):

$$f = k\varepsilon \qquad\qquad\qquad [3.3]$$

This, in turn, defines a linear relationship between transformation rate and plastic strain rate. Here plastic flow will occur at the applied stress for which the combined (chemical and mechanical) driving force is sufficient to make the rate of transformation plasticity match the imposed strain rate; yielding in a constant strain-rate tensile test then corresponds to an imposed rate of stress-assisted isothermal transformation, with kinetic behavior predictable from transformation kinetic theory.

3.3.2 Mechanism of strain-induced transformations

The kinetics of strain-induced martensitic nucleation at observed shear-band intersections can be adequately described by a simple relationship containing two temperature-dependent parameters and a fixed exponent (Olson and Cohen, 1975):

$$f^{\alpha'} = 1 - \exp\{-\beta[1 - \exp(-\alpha\varepsilon)]^n\} \qquad\qquad [3.4]$$

The first parameter (α) describes the rate of shear-band formation with respect to strain and is principally dependent on stacking-fault energy. The second parameter (β) is linearly related to the probability that a shear-band intersection will generate a martensitic embryo, and is governed by the chemical driving force for the martensitic reaction $\Delta G^{\gamma \to \alpha'}$, where γ refers to austenite and α' refers to the martensite. The transformation curve (volume fraction of martensite vs. plastic strain) is sigmoidal in shape and approaches a saturation value determined by the β parameter. The transformation rate (relative to plastic strain) is controlled by both parameters. The temperature sensitivity of these transformation kinetics arises largely through $\Delta G^{\gamma \to \alpha'}$ and the stacking-fault energy, and may be minimized by a reduction of the entropy differences, $\Delta S^{\gamma \to \alpha'}$ and $\Delta S^{\gamma \to \varepsilon}$.

3.4   Transformation plasticity constitutive relations and applications

The large transformation plasticity accompanying martensitic transformation allows substantial alteration of mechanical behavior under monotonic as well as cyclic loading conditions. A dramatic illustration of the potential of this is given by the original high-strength fully austenitic TRIP (transformation-induced plasticity) steels studied in the 1960s (Zackay *et al.*, 1967), which exhibit an extraordinary combination of strength, ductility, and toughness.

Transformation plasticity provides a significant departure from the classical view of structure/property relationships in materials. The traditional role of transformation kinetics is in the control of materials processing to achieve desired properties associated with the structure of the transformation product. Via transformation plasticity, one can design metastable materials to exploit the properties of the transformation itself, i.e., properties of structural change. Under these circumstances, knowledge of transformation kinetics can be directly applied to the prediction of the constitutive flow relations underlying observed macroscopic mechanical behavior of materials during service as well as during processing.

3.4.1   Constitutive flow relations of transformation plasticity

Detailed comparison of stress vs. strain and fraction transformed martensite vs. strain curves of TRIP steels reveals two major factors controlling the plastic-flow behavior during deformation-induced martensitic transformation (Olson and Azrin, 1978). In addition to the well-known static hardening contribution of the transformation product, a dynamic softening contribution arises from the operation of the transformation as a deformation mechanism. The latter effect is most amenable to quantitative treatment in the case of the stress-assisted transformation at sufficiently low temperatures (stresses) where plastic flow is entirely controlled by the transformation kinetics.

For barrierless martensitic nucleation controlled by interfacial mobility, time-dependent isothermal transformation can be predicted from the aforementioned thermal component of solution hardening, for which the activation energy Q can be approximated as a linear function of the acting total thermodynamic driving force,

$$Q = A + B\Delta G \qquad\qquad [3.5]$$

Following the basic kinetic theory of Pati and Cohen (1969), the initial rate of transformation $\dot{f}$ can then be expressed as

$$\dot{f} = n_s V v \exp\left(-\frac{A + B\Delta G}{RT}\right) \tag{3.6}$$

where n_s is the density of nucleation sites, V is the instantaneous mean martensitic volume, and v is the nucleation attempt frequency. The critical ΔG required to achieve a given $\dot{f}$ is then given by

$$\Delta G_{crit}(\dot{f}) = -\frac{1}{B}\left(A + RT \ln \frac{\dot{f}}{n_s V v}\right) \tag{3.7}$$

which shows a linear dependence on temperature, T. For stress-assisted transformation, where yielding occurs by the rate of transformation plasticity matching the imposed strain rate, this corresponds to an imposed transformation rate of $\dot{f} = k\dot{\varepsilon}$. Calculation of the total thermodynamic driving force (chemical plus stress contributions) at the yield stress observed (Olson and Azrin, 1978) at temperatures below M_s^σ for high-strength TRIP steels verifies the linear $\Delta G_{crit}(T)$ relation of Eq. [3.7] (Olson and Cohen, 1982). This linear relationship then predicts the critical stress for stress-assisted transformation σ_t determined by the solid curve of Fig. 3.4 where it is compared against measured stresses for 0.2% plastic strain and 1% transformation. In contrast to
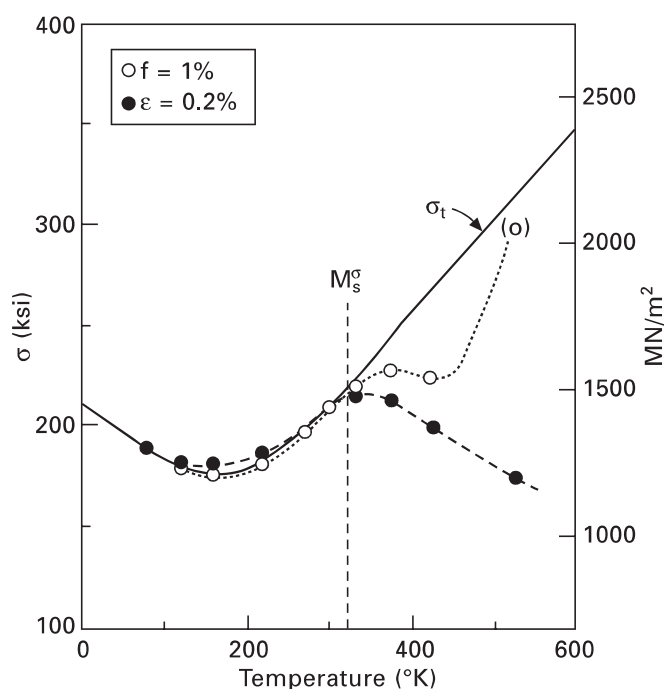
3.4 Observed temperature dependence of 0.2% yield stress and stress at which 1% martensite is detected in high-strength TRIP steel (Olson and Azrin, 1978). Solid curve (σ_t) represents theoretical (tensile) stress for stress-assisted transformation (Olson and Cohen, 1982).

the linear behavior represented in Fig. 3.3, $\sigma_t(T)$ is in this case a curve which passes through a minimum at 158 K. The curvature arises from nonlinearity of $\Delta G_{ch}(T)$ at low temperatures, and the minimum is consistent with the behavior of relatively stable alloys which exhibit suppressible isothermal ('C-curve') transformation kinetics. In the stress-assisted regime, Eqs [3.3] and [3.7] also predict a strain-rate sensitivity of flow stress of the form (Olson and Cohen, 1982):

$$\frac{\partial \sigma}{\partial \ln \dot{\varepsilon}} = -\frac{RT}{B \frac{\partial \Delta G}{\partial \sigma}} \qquad [3.8]$$

In line with the close relation between B and the activation volume for slip, the rate sensitivity of transformation plasticity is very similar to that for conventional plastic deformation.

Application of transformation plasticity to enhancement of uniform ductility and fracture toughness involves very different stress states, which must be taken into account in optimizing transformation stability for desired properties. A strong stress-state dependence of the Patel–Cohen work term (Patel and Cohen, 1953) arises from the transformation dilatation. Using the $\partial \Delta G / \partial \sigma$ values determined for uniaxial compression, uniaxial tension, and elastic crack tip, the corresponding σ_t curves calculated for the alloy of Fig. 3.4 are compared in Fig. 3.5. Also shown are 0.2% yield stress measurements for uniaxial compression. An unusually large strength-differential (S-D) effect, comparing flow stress in compression and tension, is expected in the stress-assisted regime. Although an anomalous reverse S-D effect is observed near 300 K, the expected effect is observed at low temperatures, suggesting that flow is controlled by transformation in tension and slip in compression. The prediction for the crack-tip case suggests that transformation will control flow over a wider temperature range and that the effective flow stress near 300 K is significantly reduced relative to uniaxial tension. As will be discussed further, this stress-state sensitivity is important to the achievement of improved strength/toughness combinations, allowing a high tensile strength material to benefit from the crack-tip plasticity of a softer material.

A knowledge of the kinetics of isothermal martensitic transformations can also be used to predict the shape of the σ-ε curve during stress-assisted transformation by taking into account the variation in the number of nucleation sites (n_s in Eq. [3.7]) with progress of the transformation (Olson and Cohen, 1982). The Pati–Cohen model, which satisfactorily accounts for the course of stress-free isothermal martensitic transformation, describes the nucleation-site density by an expression of the form (Pati and Cohen, 1969; Raghavan and Cohen, 1971):

$$n_s = (n_i + pf - N_v)(1 - f) \qquad [3.9]$$
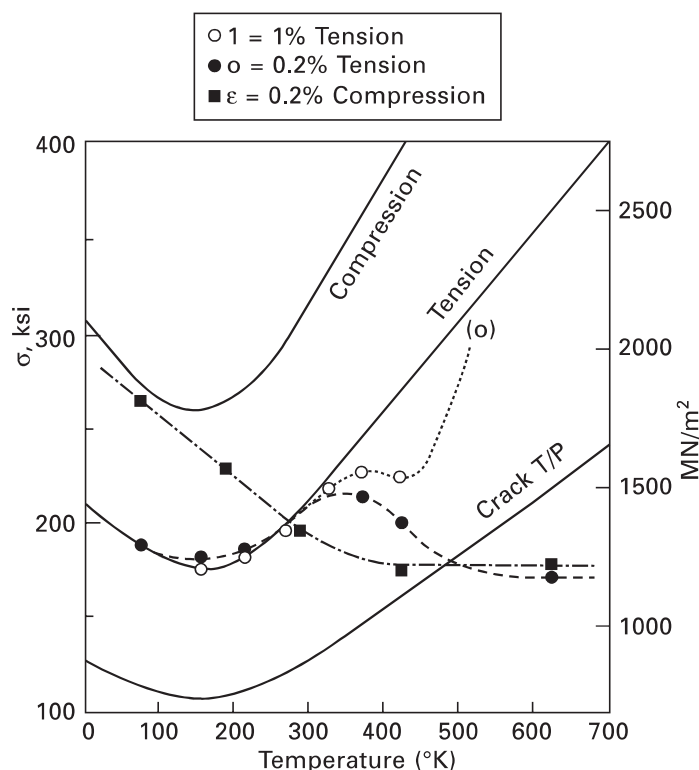
3.5 Calculated transformation stresses and measured yield stresses for the TRIP steel of Fig. 3.4 under different stress states (Olson and Cohen, 1982).

Here n_i is the initial-site density, p is an 'autocatalytic factor' accounting for new sites produced during transformation, and N_v is the number of martensitic plates per unit volume (accounting for sites which have already operated); the $(1-f)$ factor takes into account potential sites which have been 'swept up' by transformation. While the p factor can cause n_s to increase in the initial stages of transformation, a decreasing average plate volume $\overline{V}$ due to 'partitioning' can cause the $-N_v$ term to reduce n_s at later stages. A saturation level of transformation is reached when $n_s \to 0$. Substituting Eq. [3.9] into Eq. [3.7], the flow stress during stress-assisted transformation can be expressed as (Olson and Cohen, 1982):

$$\sigma_t(T, \dot{f}, \blacksquare) = -\left(B \, \frac{\partial \Delta G}{\partial \sigma} \right)^{-1} \left[A + B\Delta G_{c\blacksquare} + RT \, \ln\left(\frac{\dot{f}}{(n_\blacksquare + p^f \underline{\quad} N_v)(1 - f \blacksquare Vv)} \right) \right]$$

[3.10]

Substitution of Eq. [3.3] then provides a complete constitutive relation for $\sigma_t(\varepsilon, \dot{\varepsilon} T)$. The shape of the σ-ε curve is determined by the behavior of the denominator in the last term of Eq. [3.13]. The yield stress is controlled by n_i, a stress drop is produced by the pf autocatalytic term, and approach to saturation

causes rapid hardening as site depletion brings the denominator toward zero. Using the A and B parameters defined by the temperature dependence of σ_t in Fig. 3.4, and typical experimental values of the other kinetic parameters, a calculated σ-ε curve is compared with that measured at 158 K for the same TRIP steel in Fig. 3.6. The yield drop and flat portions of the curves are in good agreement, but the calculated final hardening (saturation) stage is too abrupt. This arises from the approximation of a singly activated process. As described earlier, the distribution of nucleation-site potencies is known to give a distribution of nucleation activation energies (Magee, 1971; Lin *et al.*, 1992), and this can account for a more gradual approach to saturation. It is important to note that the flow stresses depicted in Fig. 3.6 are all well below the stress for general yielding by slip. Relative to the 'normal' slip-controlled flow behavior of this material, the phenomena thus far considered are entirely 'softening' contributions. The high strain hardening associated with the saturation stage is best understood as the cessation of a softening phenomenon rather than the onset of a hardening mechanism. Once the transformation plasticity phenomenon (dynamic softening) associated with stress-assisted transformation is essentially complete, the higher strength of the transformation product makes its 'static hardening' contribution to the flow stress.

While control of plasticity by transformation kinetics allows rather precise prediction of flow behavior in the stress-assisted transformation regime, the
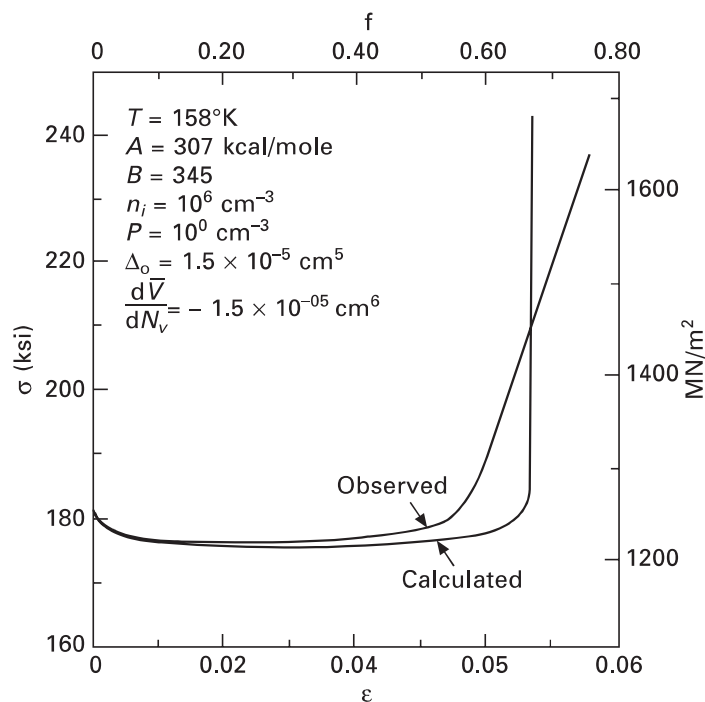
3.6 Comparison of calculated and observed (Olson and Azrin, 1978) true σ-ε curves for the TRIP steel of Fig. 3.4 (Olson and Cohen, 1982).

simultaneous operation of general slip and transformation in the strain-induced regime makes the quantitative treatment of flow behavior more difficult. Although much attention has been given to the static-hardening aspects of the two-phase mixture formed during strain-induced transformation, careful comparison of σ-ε curves has demonstrated that dynamic softening is also an important contribution. A detailed study of the transformation and flow behavior of a metastable austenitic stainless steel, summarized in Fig. 3.7, has allowed a quantitative separation of the static hardening and dynamic softening contributions during strain-induced transformation (Narutani *et al.*, 1982). The measured σ-ε curve of the metastable steel is labeled σ_{exp}. The dashed $\sigma_{\alpha'}$ and σ_{γ} curves represent the corresponding σ–ε curves of the martensite and stable austenite measured separately on specially designed similar steel compositions. One estimate of the static hardening behavior of the two-phase mixture is obtained from a simple 'rule of mixtures' using the $\sigma_{\alpha'}(\varepsilon)$, $\sigma_{\gamma}(\varepsilon)$ data and the measured $f(\varepsilon)$ curve shown at the bottom of the
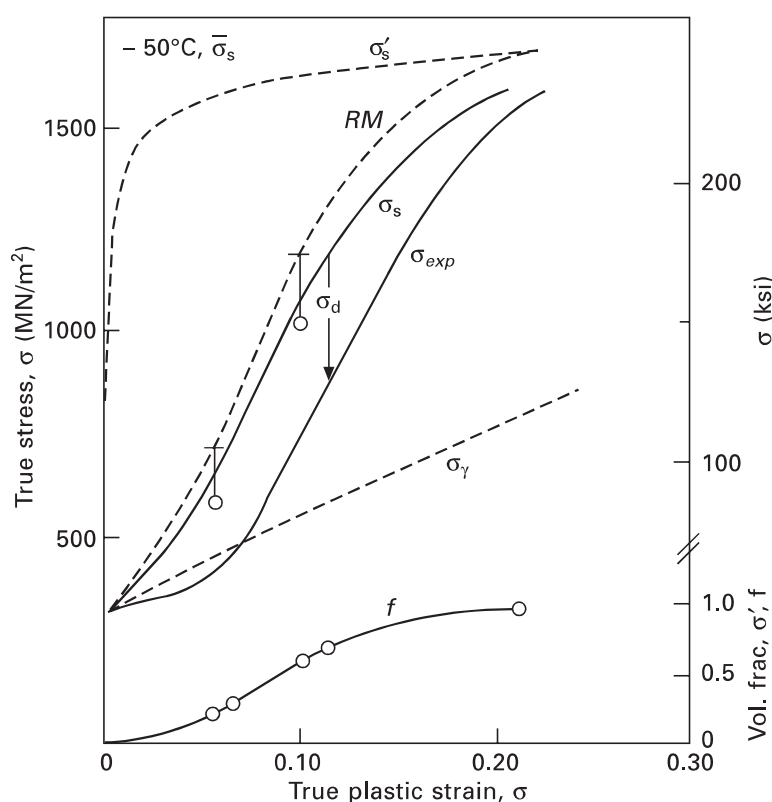
3.7 Experimental flow stress, σ_{exp}, and volume fraction martensite, *f*, vs. plastic strain, ε, for metastable austenitic steel at –50°C, $\dot{\varepsilon}$, = 2.2 × 10^{-4} s^{-1}. Dashed curves represent the stable austenite flow stress, σ_{γ}, the martensite flow stress, σ_{α}', and the prediction of the rule of mixtures for two-phase hardening, *RM*. Solid curve, σ_s, is a prediction of strain-corrected rule-of-mixtures model (Narutani *et al.*, 1982).

figure; this estimate is depicted by the dashed curve labeled *RM*. Because the transformation plasticity contribution arising from biasing of the transformation shape strain does not contribute to the strain in either phase, the *RM* curve represents an upper limit to the static-hardening behavior. A strain-corrected rule of mixtures is obtained using $\sigma_{\alpha'}$ and σ_γ values at a strain of $\varepsilon - \alpha f$, where αf corrects for the shape-strain contribution to the measured ε. An upper-limit estimate of the α coefficient is $\alpha = k^{-1}$, taking k from the measured stress-assisted transformation behavior at low temperatures. This gives the solid curve depicted just below the dashed *RM* curve. The open points represent static flow-stress estimates determined by prestrain experiments. After the transforming material had been deformed to a particular strain, the static flow stress of the resulting two-phase mixture (in the absence of dynamic transformation softening) was determined from its flow stress subsequently measured at a higher temperature where the austenite is stable, correcting for its temperature dependence. These estimates and the *RM* estimate bracket the strain-corrected rule of mixtures estimate which is therefore taken as a reasonable approximation of the flow stress arising from static hardening, σ_s. This is expressed as:

$$\sigma_s = [1 - f] \cdot \sigma_\gamma(\varepsilon - \alpha f) + f \cdot \sigma_{\alpha'}(\varepsilon - \alpha f) \qquad [3.11]$$

As indicated in Fig. 3.7, the dynamic softening increment $\Delta\sigma_d$ is then taken as the difference between σ_s and σ_{exp}. Correlation of the $\Delta\sigma_d$ increment thus obtained with f-ε behavior observed over a wide temperature range indicates that the fractional softening increment is proportional to $df/d\varepsilon$:

$$\frac{\Delta\sigma_d}{\sigma_s} = \beta \cdot \frac{df}{d\varepsilon} \qquad [3.12]$$

where $\beta = 5.3 \times 10^{-2}$. This then gives a constitutive flow relation for strain-induced transformation of the form:

$$\sigma = \{[1 - f] \cdot \sigma_\gamma(\varepsilon - \alpha f) + f \cdot \sigma_{\alpha'}(\varepsilon - \alpha f)\} \cdot \left[1 - \beta \cdot \frac{df}{d\varepsilon}\right] \qquad [3.13]$$

Through Eq. [3.13], $\sigma(\varepsilon, \dot{\varepsilon}, T)$ can be predicted from a knowledge of f, σ_γ and $\sigma_{\alpha'}$ as functions of ε, $\dot{\varepsilon}$, and T.

As in the case of stress-assisted transformation, dynamic softening is the dominant factor at low strains, causing the flow stress σ_{exp} of the transforming material in Fig. 3.7 to fall below that of the stable austenite, σ_γ. The static hardening becomes dominant at high strains. The combined effect of these two factors delays the maximum hardening rate $d\sigma/d\varepsilon$ to a higher strain than that where $df/d\varepsilon$ is maximum. The maximum $d\sigma/d\varepsilon$ arises from both the static hardening (proportional to $df/d\varepsilon$) and the diminution of dynamic softening (proportional to $-d^2f/d\varepsilon^2$) as $df/d\varepsilon$ decreases. Again, the cessation

of a softening phenomenon provides a major contribution to the net rate of hardening. The generalization of this constitutive law to three-dimensional deformation has been developed by Stringfellow *et al.* (1992).

3.4.2   Stability of plastic flow

With constitutive flow relations for transformation plasticity based on the transformation kinetics, we may now consider the associated macroscopic flow behavior as predicted by continuum plasticity theory. The ability of transformation plasticity to dramatically alter the shape of a σ-ε curve naturally raises the question of the optimum or 'ideal' curve shape for stability of plastic flow. The minimum strain-hardening rate required to maintain stable flow during tensile deformation is expressed by (Backofen, 1972):

$$\frac{d\sigma}{d\varepsilon} = \sigma \qquad\qquad [3.14]$$

A consequence of strain hardening is that the hardening rate necessary to maintain stability is increased. Excessive hardening therefore makes it more difficult to maintain stability at higher strains. It follows that the most efficient use of a hardening increment $\Delta\sigma$ is to distribute it with respect to strain in such a way that $d\sigma/d\varepsilon$ increases with ε. The ideal hardening curve, which provides the minimum hardening rate necessary to maintain stability at all strains, is given by the solution of the differential equation represented by Eq. [3.15]:

$$\sigma = \sigma_y \exp(\varepsilon) \qquad\qquad [3.15]$$

where σ_y corresponds to the yield stress. In contrast to the usual downward curvature associated with the structural hardening and recovery processes controlling deformation by slip, the ideal flow relation of Eq. [3.15] possesses upward curvature (Kocks *et al.*, 1979). The 'delayed hardening' behavior associated with the intersection of dynamic softening and static hardening phenomena in transformation plasticity provides an effective means of increasing $d\sigma/d\varepsilon$ with ε to achieve this curvature.

   The ideal hardening behavior of Eq. [3.15] is contrasted with the conventional downward-curving behavior, approximated by a power law $\sigma = K\varepsilon^n$, in Fig. 3.8. The open circle indicates the point where the power-law curve reaches the condition for flow localization by tensile necking, i.e., where $d\sigma/d\varepsilon$ falls below σ (Eq. [3.14]). From a local viewpoint, which considers the conditions at the necking strain, one would attribute the necking to insufficient hardening, and would propose to increase uniform ductility by increasing the hardening exponent, n. From a perspective which considers the σ-ε curve as a whole, the necking can equally well be ascribed to excessive hardening at low strains. In the region where the $K\varepsilon^n$ curve lies above the $\sigma_0 \exp \varepsilon$ curve,
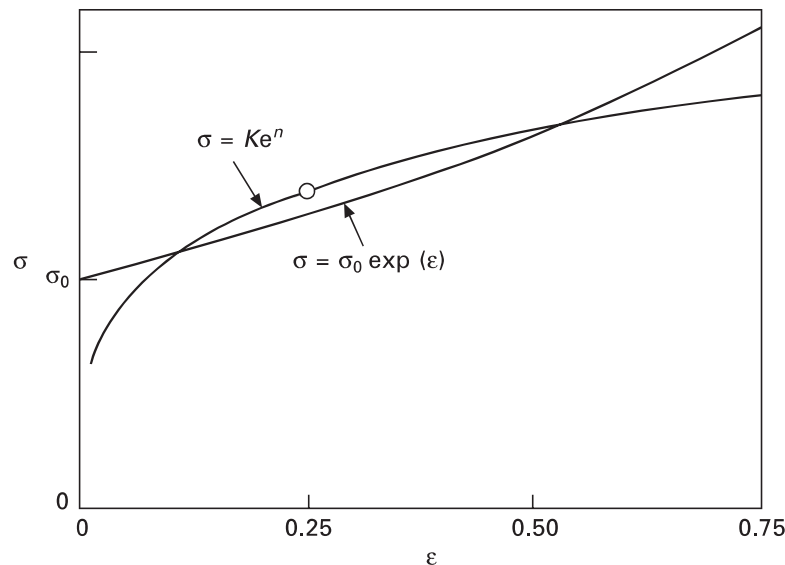
3.8 Comparison of ideal exponential hardening behavior with power-law hardening. Open point indicates necking strain.

the superposition of a *softening* mechanism which lowers the flow stress to the $\sigma_0 \exp \varepsilon$ curve would double the uniform ductility for the case depicted in Fig. 3.8. This illustrates the potential of the dynamic softening phenomenon in transformation plasticity for the enhancement of flow stability. At higher strains, where the $K\varepsilon^n$ curve falls below the $\sigma_0 \exp \varepsilon$ curve, superposition of a hardening mechanism, such as the high-strain static hardening contribution in transformation plasticity, is required to further maintain stable flow. If the ideal $\sigma_0 \exp \varepsilon$ curve is followed, necking will never occur, and uniform ductility will be controlled by fracture rather than plastic instability. Figure 3.8 illustrates that the dynamic softening contribution to transformation plasticity at lower strains can be equally important as the high-strain static hardening contribution in promoting stability of plastic flow.

3.4.3   Applications of transformation plasticity to ductility

The flow-stabilizing influence of the σ-ε curve-shaping effects associated with transformation plasticity allows dramatic enhancement of uniform ductility under conditions of optimum thermodynamic stability, and this phenomenon is the most well-established transformation plasticity application. Although temperature sensitivity and Lüders-band behavior limit the useful ductility of the highest strength TRIP steels, which depend almost entirely on their transformation behavior for stability of flow, the flow-stabilizing contribution of a moderate rate of transformation in lower strength metastable austenitic steels has been practically applied for many years. Control of transformation plasticity has led to the development of numerous commercial high-formability stainless steels.

The enhancement of flow stability in metastable austentic steels via transformation plasticity has been extensively investigated (Krivobok and Talbot, 1950; Angel, 1954; Fiedler *et al.*, 1955; Powell *et al.*, 1958; Bressanelli and Moskowitz, 1966; Zackay *et al.*, 1967; Tamura *et al.*, 1970; Olson and Azrin, 1978; Zackay *et al.*, 1978; Hecker *et al.*, 1982), and analyzed in terms of Eq. [3.15] (Azrin *et al.*, 1976). A continuous local strain measurement technique allowed determination of true stress–true strain behavior of the original high-strength austenitic TRIP steels during both uniform and localized plastic flow under a variety of conditions (Azrin *et al.*, 1976; Olson and Azrin, 1978, unpublished research). Figure 3.9 summarizes such curves obtained for uniaxial tensile deformation of a fully austenitic TRIP steel of nominal composition Fe-9Cr-8Ni-4Mo-2Si-2Mn-0.3C strengthened by warm working to a 60% reduction at 450°C (Olson and Azrin, 1978). Arrows indicate the necking strain or uniform strain, ε_u. The temperature (stability) dependence of the strength and ductility properties is summarized in Fig. 3.10. Consistent with the constitutive model predictions, the true σ-ε curves in Fig. 3.9 have a characteristic sigmoidal shape. The temperature dependence of the 0.2% yield strength σ_y in Fig. 3.10 is similar to that of Fig. 3.4, indicating an M_s^σ temperature near 280 K. The ultimate tensile strength (UTS) reaches a maximum in the stress-assisted transformation regime, limited at lower temperatures by fracture. The latter effect is indicated by the intersection of uniform strain ε_u and the fracture strain ε_f at the lowest
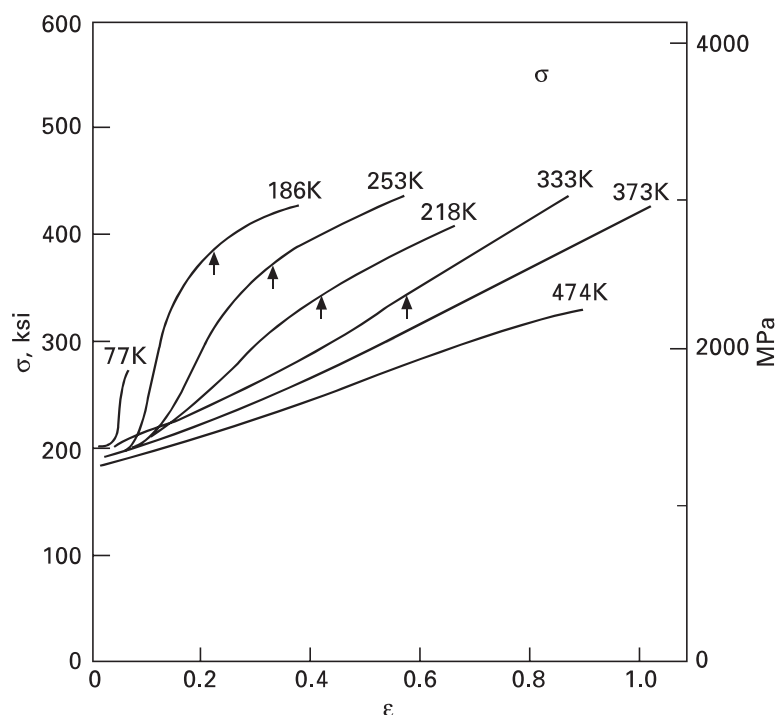
3.9 True stress–strain curves of high-strength austenitic TRIP steel. Arrows indicate necking strain (Olson and Azrin, 1978).
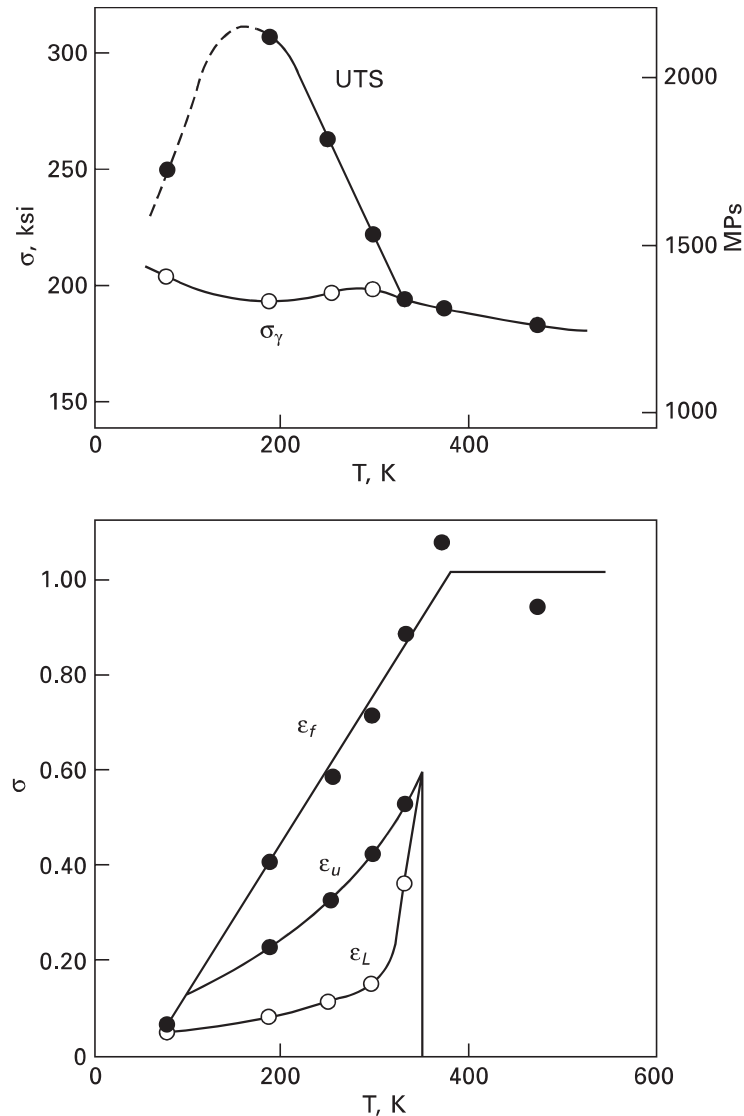
3.10 Tensile properties of austenitic TRIP steel of Fig. 3.9, including Lüders strain ε_L, uniform (necking) strain ε_u, and fracture strain ε_f.

temperature. The uniform ductility ε_u reaches a maximum above M_s^σ at a temperature near 350 K, reflecting an optimum overall rate of deformation-induced transformation. As indicated by the shape of the σ-ε curves, early completion of transformation at lower temperatures leads to early necking in the downward-curving portion of the σ-ε behavior that follows. Above 350 K the strain hardening associated with a reduced degree of transformation is insufficient to maintain stable flow in this high-strength material, and the uniform ductility is negligible. The existence of such an optimum stability for maximum uniform ductility in metastable austenitic steels in general is well established (Bressanelli and Moskowitz, 1966; Tamura *et al*., 1970; Zackay *et al*., 1978). The shape of the optimum stability 333 K curve in

Fig. 3.9, giving a uniform ductility of 60% with a yield strength of 200 ksi (1.4 GPa), is quite close to the ideal exponential form.

3.4.4   Applications of transformation plasticity to fracture toughness

Transformation toughening in austenitic steels is complicated both by the greater complexity of the constitutive behavior of strain-induced as opposed to stress-assisted transformation, and the more complex processes of ductile fracture. The experimental study by Léal (1984) of the interaction of transformation with ductility and fracture toughness is reviewed in Olson and Cohen (1986b). A series of six precipitation-hardenable austenitic steels based on A286 steel were designed to have a constant 1300 MPa yield strength, varying stability with respect to transformation, and a varying transformation volume change. The alloys also had a fairly strong temperature dependence of phase stability to allow variation of stability over wide limits. The fracture ductility and J_{IC} toughness were found to peak at the M_s^{σ} of their respective stress states.

A subsequent study by Young (1988), reviewed in Olson (1990), involved a thorough evaluation of the transformation kinetics and constitutive relations of phosphocarbide-strengthened austenitic steels in which the transformation volume change and austenite-martensite hardness difference could both be varied. The measured enhancement of toughness and fracture ductility in these alloys was similar to that observed by Léal. In the regime of shear instability controlled ductile fracture, the increase in J_{IC} toughness varies linearly with the height of the transformation zone at the crack front. Correlation of the slope of this toughening response with transformation volume change $\delta V/V$, and austenite-martensite hardness differences δH_v (influencing strain hardening) shows that, in contrast to brittle solids, the toughening behavior is more dilatation sensitive, with the $\delta J/h$ scaling with the third power of $\delta V/V$. Higher δH_v also promotes more toughening.

The remarkable transformation toughening observed by Stavehaug (1990) in a more recent series of γ'-strengthened austenites is summarized in Fig. 3.11, which plots the measured room-temperature J_{IC} toughness vs. a thermodynamic stability parameter defined by the difference between the total acting thermodynamic driving force and its critical value at M_s^{σ}. Similar to the results of Léal and Young, the toughening is maximum at the M_s^{σ} condition, but in these experiments the apparent toughness enhancement over the stable austenite toughness indicated by the dashed line is significantly higher.

Quantitative modeling of the mechanics of the transformation toughening has addressed mechanisms on two length scales. As an analysis of interactions of transformation hardening and void softening induced localization at the
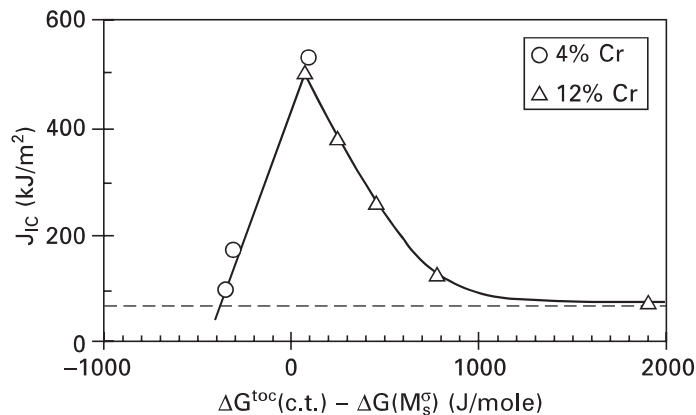
3.11 Measured J_{IC} fracture toughness of 12Cr and 4Cr austenitic alloy series (1380 MPa yield strength) as a function of thermodynamic austenite stability parameter (Stavehaug, 1990).

macroscopic level, Stringfellow and Parks (1991) and Stringfellow (1990) performed a series of model calculations incorporating a void softening model into the transformation constitutive model.

On a finer length scale, electron microscopy observations (Young, 1988) of the distribution of fine strain-induced martensite around 0.1 μm scale particles after straining to levels beyond the microvoid nucleation strain of non-transforming material indicate a more direct cross-interaction between transformation and the unit process of ductile fracture. Socrate and Parks (Socrate, 1995) have applied the transformation constitutive model in numerical simulations of microvoid nucleation, growth and coalescence employing a cohesive-zone model for interface debonding similar to that introduced by Needleman (1987). Using interfacial strength estimates for the TiC particles observed in the experimental alloys, Fig. 3.12 shows the computed stress–strain curves for a cell model of the crack-tip process zone with a remote stress state of $\sigma_h/\overline{\sigma} = 1.12$. Dotted, dashed, and solid curves represent material with (a) pre-existing void, (b) a permanently bonded particle, and (c) a debonding particle, respectively. The curves labeled with a T depict the effect of strain-induced transformation at a stability near that of the crack-tip M_s^σ temperature. Comparing the transforming and non-transforming behaviors for material with either a pre-existing void or a debonding particle, transformation greatly delays the onset of microvoid softening based negative strain hardening that drives shear localization fracture. Computed transformation fields prior to nucleation are in good agreement with the experimental observations. Simulations of interacting pairs of particles also demonstrate retardation of microvoid coalescence, but the largest toughening effect appears to be associated with delay of shear instability driven by void growth softening. The strain corresponding to the onset of terminal softening (stress maximum) in Fig. 3.12 increases
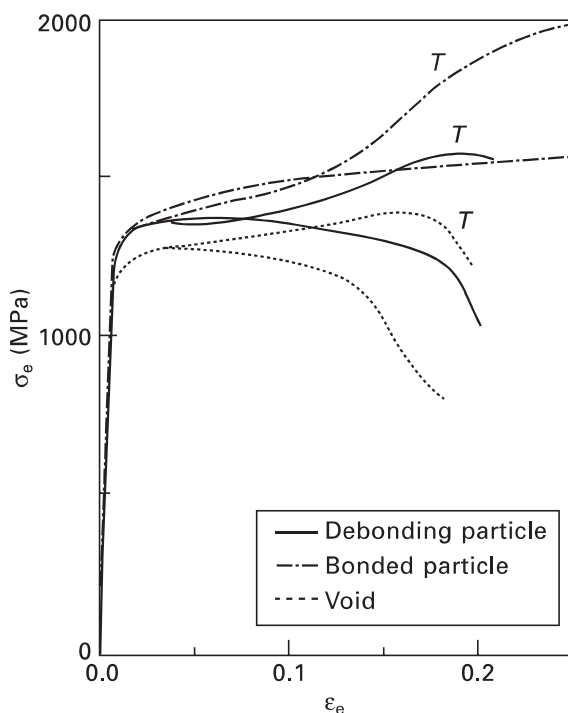
3.12 Computed stress–strain curves for crack tip cell model; curves labeled *T* represent transforming material while others represent non-transforming material (Socrate, 1995).

with transformation by a factor similar to the J_{IC} toughness enhancement of Fig. 3.11.

3.5 Conclusions

Building on dislocation-based theory of the mechanism and kinetics of heterogeneously nucleated martensitic transformations, quantitative models have been developed for the kinetics of stress-assisted and strain-induced martensitic transformations. Constitutive flow relations for transformation plasticity have been derived based on these kinetic models, incorporating the static hardening effect of the transformation product and the dynamic softening effect of the transformation as a deformation mechanism. The transformation softening and hardening effects can distort the stress–strain curve from the usual downward-curving shape to an upward-curving shape which approximates an ideal exponential hardening behavior promoting maximum uniform ductility. Numerical simulation of shear-instability-controlled ductile fracture demonstrates that the transformation plasticity behavior can also account for observed substantial enhancement of ductile fracture toughness.

The demonstrated behaviors in fully austenitic steels offer a foundation for predictive control of transformation plasticity in dispersed-phase systems.

More broadly, the application of predictive theory of transformation plasticity to enhance mechanical properties of advanced steels remains a vital avenue of steel research. Predictive control of the complexities of martensitic behavior has served as the foundation of a systems approach to science-based materials engineering. In this way, ferrous metallurgy has played a leading role in the new technology of materials design (Olson, 2006).

3.6   References

Angel, T. (1954). 'Formation of Martensite in Austenitic Stainless Steels'. *J. Iron Steel Inst*. **177**: 165–174.

Azrin, M., G. B. Olson, *et al*. (1976). 'Inhomogeneous Deformation and Strain-Rate Effects in High-Strength Trip Steels'. *Materials Science and Engineering* **23**(1): 33–41.

Backofen, W. A. (1972). *Deformation Processing*. Reading, MA: Addison-Wesley.

Bogers, A. J. and W. G. Burgers (1964). 'Partial Dislocations on the (110) Planes in the bcc Lattice and the Transition of the fcc into the bcc Lattice'. *Acta Metall*. **12**: 225–261.

Bolling, G. F. and R. H. Richman (1970). 'Influence of Stress of Martensite-Start Temperatures in Fe-Ni-C Alloys'. *Scripta Metallurgica* **4**(7): 539–544.

Bressanelli, J. P. and A. Moskowitz (1966). 'Effects of Strain Rate Temperature and Composition on Tensile Properties of Metastable Austenitic Stainless Steels.' *ASM Transactions Quarterly* **59**(2): 223–239.

Brooks, J. W., M. H. Loretto, *et al*. (1979). '*In-situ* Observations of the Formation of Martensite in Stainless-Steel'. *Acta Metallurgica* **27**(12): 1829–1838.

Christian, J.W., G. B. Olson, *et al*. (1995). 'Classification of Displacive Transformations: What is a Martensitic Transformation?', *Proc. ICOMAT 95*, supplement to *J. de Phys. III*, **5** Coll. C8: 3–10.

Fiedler, H. C., B. L. Averbach, *et al*. (1955). 'The Effect of Deformation on the Martensitic Transformation'. *Trans. ASM* **47**: 267–290.

Fisher, P. J. (1974). The Effects of Stress on the Martensite Transformation. PhD Thesis, University of New South Wales, Australia.

Ghosh, G. and G. B. Olson (1994a). 'Kinetics of Fcc→Bcc Heterogeneous Martensitic Nucleation. 1. The Critical Driving-Force for Athermal Nucleation'. *Acta Metallurgica et Materialia* **42**(10): 3361–3370.

Ghosh, G. and G. B. Olson (1994b). 'Kinetics of Fcc→Bcc Heterogeneous Martensitic Nucleation. 2. Thermal-Activation'. *Acta Metallurgica et Materialia* **42**(10): 3371–3379.

Hecker, S. S., M. G. Stout, *et al*. (1982). 'Effects of Strain State and Strain Rate on Deformation-Induced Transformation in 304 Stainless-Steel. 1. Magnetic Measurements and Mechanical-Behavior'. *Metallurgical Transactions A – Physical Metallurgy and Materials Science* **13**(4): 619–626.

Kaufman, L. and M. Cohen (1958). 'Thermodynamics and Kinetics of Martensitic Transformations'. *Prog. Metal Physics 1*: 165–246.

Kocks, U. F., J. J. Jonas, *et al*. (1979). 'The Development of Strain-Rate Gradients'. *Acta Metallurgica* **27**: 419–432.

Krivobok, V. N. and A. M. Talbot (1950). 'Effect of Temperature on the Mechanical Properties, Characteristics, and Processing of Austenitic Stainless Steels'. *Proceedings American Society for Testing and Materials* **50**: 895–930.